Finite size specimens with cracks of icosahedral Al–Pd–Mn quasicrystals*

Yang Lian-Zhi(杨连枝)[a)b)], Ricoeur Andreas[c)], He Fan-Min(何蕃民)[d)], and Gao Yang(高 阳)[a)†]

[a)] *College of Science, China Agricultural University, Beijing* 100083, *China*
[b)] *College of Engineering, China Agricultural University, Beijing* 100083, *China*
[c)] *Institute of Mechanics, University of Kassel, Kassel* 34125, *Germany*
[d)] *Sichuan Hydropower Investment & Management Group LTD, Chengdu* 611130, *China*

(Received 7 November 2013; revised manuscript received 17 December 2013; published online 18 March 2014)

Icosahedral quasicrystals are the most important and thermodynamically stable in all about 200 kinds of quasicrystals currently observed. Beyond the scope of classical elasticity, apart from a phonon displacement field, there is a phason displacement field in the elasticity of the quasicrystal, which induces an important effect on the mechanical properties of the material and makes an analytical solution difficult to obtain. In this paper, a finite element algorithm for the static elasticity of icosahedral quasicrystals is developed by transforming the elastic boundary value problem of the icosahedral quasicrystals into an equivalent variational problem. Analytical and numerical solutions for an icosahedral Al–Pd–Mn quasicrystal cuboid subjected to a uniaxial tension with different phonon–phason coupling parameters are given to verify the validity of the numerical approach. A comparison between the analytical and numerical solutions of the specimen demonstrates the accuracy and efficiency of the present algorithm. Finally, in order to reveal the fracture behavior of the icosahedral Al–Pd–Mn quasicrystal, a cracked specimen with a finite size of matter is investigated, both with and without phonon–phason coupling. Meanwhile, the geometry factors are calculated, including the stress intensity factor and the crack opening displacement for the finite-size specimen. Computational results reveal the importance of phonon–phason coupling effect on the icosahedral Al–Pd–Mn quasicrystal. Furthermore, the finite element procedure can be used to solve more complicated boundary value problems.

Keywords: icosahedral quasicrystals, finite-size crack specimen, finite element method, cuboid

PACS: 61.44.Br, 62.20.D−, 62.20.M−, 07.05.Tp **DOI:** 10.1088/1674-1056/23/5/056102

1. Introduction

Since the first discovery of icosahedral quasicrystals (QCs) in Al–Mn alloys in 1984 by Shechtman *et al.*[1] and Levine-Stcinhardt,[2] their mechanical behaviors, especially the elasticity and defects, have been investigated both experimentally and theoretically.[3–6] Based on the symmetry breaking principle of Landau, the physical basis of elasticity of the QCs has been formulated by Bak[7,8] and Levine *et al.*,[9] in which a phason displacement field is introduced along with the classical phonon displacement field. The phonon field is similar to the elastic field in traditional continuum mechanics under the condition of long-wavelength approximation, while the phason field is responsible for the rearrangements of local atomic configurations. Since the QCs at room temperature are brittle solids,[10] Ding *et al.*[11] summarized the generalized linear elasticity theory of the QCs, which provides the fundamental basis for the stress analysis of these materials.

Among more than 200 individual QCs observed to date, nearly half are icosahedral QCs, which exhibit a great thermal stability and play an important role in these kinds of materials.[10] The phonon and phason elastic material constants provide a basis for the study of the mechanical behavior of these materials. The constants of several icosahedral QCs, such as Al–Pd–Mn alloys, have been experimentally measured through various methods, such as the X-ray diffraction and neutron scattering.[12–14] However, the coupling elastic constants are very difficult to measure,[15] and have always been estimated empirically.

The analytical solutions for the plane or three-dimensional (3D) problems of QCs with dislocations or cracks in an infinite space have been obtained by means of Green's function method,[16,17] the displacement potential method,[18–20] the perturbation method,[21] the Fourier analysis, the complex variable function-conformal mapping method,[22,23] etc. However, for 3D icosahedral QCs, due to a large number of field variables and field equations involved in the elasticity of this matter, the only available analytical solutions are for the plane problems. Furthermore, there are tremendous difficulties in obtaining analytical solutions for the 3D complex crack problems of these QCs with finite sizes. Therefore, it is necessary to develop numerical methods to handle these problems.

*Project supported by the National Natural Science Foundation of China (Grant No. 11172319), the Scientific Fund of Chinese Universities (Grant Nos. 2011JS046 and 2013BH008), the Opening Fund of State Key Laboratory of Nonlinear Mechanics, Program for New Century Excellent Talents in University, China (Grant No. NCET-13-0552), and the National Science Foundation for Post-doctoral Scientists of China (Grant No. 2013M541086).

†Corresponding author. E-mail: gaoyangg@gmail.com

© 2014 Chinese Physical Society and IOP Publishing Ltd

Numerical methods, such as the molecular dynamic method, the finite difference method, and the mesh-free method, the finite element method, have in general been used to solve complex boundary value problems. The molecular dynamic method[24] has been used to simulate the 3D mechanical behaviors of icosahedral QCs. The finite difference method[25] has also been adopted to solve the plane dynamic problems of icosahedral QCs. The mesh-free method was applied by Sladek *et al.*[26,27] to analyze the bending and crack in 1D orthorhombic and 2D decagonal QCs under both static and transient dynamic loads. The finite element method for QCs was first deduced by Fan[10] to solve the two-dimensional (2D) problems of 2D QCs. However, up to now, a finite element method has not been developed for icosahedral QCs.

In this paper, a finite element algorithm for the static elasticity of icosahedral QCs is developed by transforming the elastic boundary value problem of icosahedral QCs into an equivalent variational problem of an energy functional. Analytical and numerical solutions for an icosahedral Al–Pd–Mn QC cuboid subjected to a unaxial tension are derived to verify the validity of the numerical approach. Finally, a cracked thin icosahedral Al–Pd–Mn QC plate with a finite size is investigated to reveal the fracture behavior of the specimen.

2. Basic equations

Within the theory of elasticity of QCs,[11] displacement vectors are denoted as $\boldsymbol{u}(\boldsymbol{x})$ in the phonon field and $\boldsymbol{w}(\boldsymbol{x})$ in the phason field, both of which depend on the coordinate $\boldsymbol{x}$ in real space. The phonon strain ε_{ij} and phason strain w_{ij} of an icosahedral QC are given by

$$\varepsilon_{ij} = (\partial_j u_i + \partial_i u_j)/2, \quad w_{ij} = \partial_j w_i, \tag{1}$$

where $\partial_j = \partial/\partial x_j$, and the subscripts $i, j = 1,2,3$.

The phonon stress σ_{ij} and phason stress H_{ij} are, respectively, given by the generalized Hooke's Law[11] in the following form:

$$\sigma_{ij} = C_{ijkl}\varepsilon_{kl} + R_{ijkl}w_{kl}, \quad H_{ij} = R_{klij}\varepsilon_{kl} + K_{ijkl}w_{kl}, \tag{2}$$

where $k,l = 1,2,3$. All subscripts satisfy the sum convention. C_{ijkl} and K_{ijkl}, respectively, denote the phonon and phason elastic constants, and R_{ijkl} are the phonon–phason coupling elastic constants. For an icosahedral QC, these elastic tensors are described as[28]

$$\begin{aligned} C_{ijkl} &= \lambda\delta_{ij}\delta_{kl} + \mu\left(\delta_{ik}\delta_{jl} + \delta_{il}\delta_{jk}\right), \\ K_{ijkl} &= K_1\delta_{ik}\delta_{jl} + K_2\left(\delta_{ij}\delta_{kl} - \delta_{il}\delta_{jk}\right), \\ R_{ijkl} &= R\left(\delta_{(i)1} - \delta_{(i)2}\right)\left(\delta_{ij}\delta_{kl} - \delta_{ik}\delta_{jl} + \delta_{il}\delta_{jk}\right), \end{aligned} \tag{3}$$

where λ and μ are Lamé constants with the same definitions as that of crystals, K_1 and K_2 are phason elastic constants, and R is the coupling constant. According to Eq. (2), the explicit relations between stresses and strains are given by

$$\begin{aligned}
\sigma_{11} &= \lambda\theta + 2\mu\varepsilon_{11} + R(w_{11} + w_{22} + w_{33} + w_{13}), \\
\sigma_{22} &= \lambda\theta + 2\mu\varepsilon_{22} - R(w_{11} + w_{22} - w_{33} + w_{13}), \\
\sigma_{33} &= \lambda\theta + 2\mu\varepsilon_{33} - 2Rw_{33}, \\
\sigma_{23} &= \sigma_{32} = 2\mu\varepsilon_{23} + R(w_{32} - w_{12} - w_{21}), \\
\sigma_{31} &= \sigma_{13} = 2\mu\varepsilon_{31} + R(w_{11} - w_{22} + w_{31}), \\
\sigma_{12} &= \sigma_{21} = 2\mu\varepsilon_{12} + R(w_{21} - w_{23} - w_{12}), \\
H_{11} &= R(\varepsilon_{11} - \varepsilon_{22} + 2\varepsilon_{31}) + K_1 w_{11} + K_2(w_{31} + w_{13}), \\
H_{22} &= R(\varepsilon_{11} - \varepsilon_{22} - 2\varepsilon_{31}) + K_1 w_{22} + K_2(w_{13} - w_{31}), \\
H_{33} &= R(\varepsilon_{11} + \varepsilon_{22} - 2\varepsilon_{33}) + (K_1 + K_2)w_{33}, \\
H_{23} &= -2R\varepsilon_{12} + (K_1 - K_2)w_{23} + K_2(w_{12} - w_{21}), \\
H_{31} &= 2R\varepsilon_{31} + (K_1 - K_2)w_{31} + K_2(w_{11} - w_{22}), \\
H_{12} &= -2R(\varepsilon_{23} + \varepsilon_{12}) + K_1 w_{12} + K_2(w_{23} + w_{32}), \\
H_{32} &= 2R\varepsilon_{23} + (K_1 - K_2)w_{32} - K_2(w_{12} + w_{21}), \\
H_{13} &= R(\varepsilon_{11} - \varepsilon_{22}) + (K_1 - K_2)w_{13} + K_2(w_{11} + w_{22}), \\
H_{21} &= 2R(\varepsilon_{12} - \varepsilon_{23}) - K_2(w_{23} + w_{32}) + K_1 w_{21},
\end{aligned} \tag{4}$$

where $\theta = \varepsilon_{11} + \varepsilon_{22} + \varepsilon_{33}$ denotes the volume strain. The strain components are arranged in a vector, as follows:

$$\begin{aligned}
\begin{pmatrix} \varepsilon_{ij} \\ w_{ij} \end{pmatrix} = \{&\varepsilon_{11}, \varepsilon_{22}, \varepsilon_{33}, \gamma_{23}, \gamma_{31}, \gamma_{12}, w_{11}, w_{22}, w_{33}, \\
&w_{23}, w_{31}, w_{12}, w_{32}, w_{13}, w_{21}\}^{\mathrm{T}},
\end{aligned} \tag{5}$$

where the superscript T represents the transpose, $\gamma_{ij} = 2\varepsilon_{ij}$ $(i \neq j)$, and the stress components of the same order are expressed as

$$\begin{aligned}
\begin{pmatrix} \sigma_{ij} \\ H_{ij} \end{pmatrix} = \{&\sigma_{11}, \sigma_{22}, \sigma_{33}, \sigma_{23}, \sigma_{31}, \sigma_{12}, H_{11}, H_{22}, H_{33}, H_{23}, \\
&H_{31}, H_{12}, H_{32}, H_{13}, H_{21}\}^{\mathrm{T}}.
\end{aligned} \tag{6}$$

Equation (4) can be transformed into

$$\begin{pmatrix} \sigma_{ij} \\ H_{ij} \end{pmatrix} = [\boldsymbol{D}] \begin{pmatrix} \varepsilon_{ij} \\ w_{ij} \end{pmatrix}, \tag{7}$$

where $[\boldsymbol{D}]$ is a 15×15 symmetric elastic constant matrix, that is,

$$[\boldsymbol{D}] = \begin{bmatrix} [\boldsymbol{C}] & [\boldsymbol{R}] \\ [\boldsymbol{R}]^{\mathrm{T}} & [\boldsymbol{K}] \end{bmatrix}, \tag{8}$$

where

$$[\boldsymbol{C}] = \begin{bmatrix} \lambda+2\mu & \lambda & \lambda & 0 & 0 & 0 \\ \lambda & \lambda+2\mu & \lambda & 0 & 0 & 0 \\ \lambda & \lambda & \lambda+2\mu & 0 & 0 & 0 \\ 0 & 0 & 0 & \mu & 0 & 0 \\ 0 & 0 & 0 & 0 & \mu & 0 \\ 0 & 0 & 0 & 0 & 0 & \mu \end{bmatrix},$$

$$[\boldsymbol{R}] = \begin{bmatrix} R & R & R & 0 & 0 & 0 & 0 & R & 0 \\ -R & -R & R & 0 & 0 & 0 & 0 & -R & 0 \\ 0 & 0 & -2R & 0 & 0 & 0 & 0 & 0 & 0 \\ 0 & 0 & 0 & 0 & 0 & -R & R & 0 & -R \\ R & -R & 0 & 0 & R & 0 & 0 & 0 & 0 \\ 0 & 0 & 0 & -R & 0 & -R & 0 & 0 & R \end{bmatrix},$$

$$[\boldsymbol{K}]=\begin{bmatrix} K_1 & 0 & 0 & 0 & K_2 & 0 & 0 & K_2 & 0 \\ 0 & K_1 & 0 & 0 & -K_2 & 0 & 0 & K_2 & 0 \\ 0 & 0 & K_1+K_2 & 0 & 0 & 0 & 0 & 0 & 0 \\ 0 & 0 & 0 & K_1-K_2 & 0 & K_2 & 0 & 0 & -K_2 \\ K_2 & -K_2 & 0 & 0 & K_1-K_2 & 0 & 0 & 0 & 0 \\ 0 & 0 & 0 & K_2 & 0 & K_1 & -K_2 & 0 & 0 \\ 0 & 0 & 0 & 0 & 0 & -K_2 & K_1-K_2 & 0 & -K_2 \\ K_2 & K_2 & 0 & 0 & 0 & 0 & 0 & K_1-K_2 & 0 \\ 0 & 0 & 0 & -K_2 & 0 & 0 & -K_2 & 0 & K_1 \end{bmatrix}.$$

The balance laws require that

$$\partial_j\sigma_{ij}+f_i=0, \partial_j H_{ij}+g_i=0, \tag{9}$$

where f_i and g_i are, respectively, the body forces in the phonon and phason fields.

The domain of the boundary value problem is denoted as Ω. The $\Gamma_{\rm t}$ and $\Gamma_{\rm u}$ denote the stress and displacement that determine the Neumann and Dirichlet boundaries, respectively. The above formulae are then defined in any interior point of the domain Ω. At the boundary $\Gamma_{\rm t}$, the stresses satisfy the following boundary conditions:[10]

$$\begin{cases} \sigma_{ij}n_j=T_i, \\ H_{ij}n_j=h_i, \end{cases} \quad (x_1,x_2,x_3)\in\Gamma_{\rm t}. \tag{10}$$

At the boundary $\Gamma_{\rm u}$, the displacements satisfy the following boundary conditions:[10]

$$\begin{cases} u_i=\bar{u}_i, \\ w_i=\bar{w}_i, \end{cases} \quad (x_1,x_2,x_3)\in\Gamma_{\rm u}, \tag{11}$$

where T_i is the traction vector in the phonon field, h_i is the generalized traction vector in the phason field at the boundary $\Gamma_{\rm t}$, n_j is the unit outward normal vector at any point of the boundary $\Gamma_{\rm t}$, and $\bar{u}_i$ and $\bar{w}_i$ are the given displacements at the boundary $\Gamma_{\rm u}$. According to Eq. (9), only static problems are studied, and the initial value problems will not be considered.

3. Finite element formulation for the static elasticity of QCs

The variational principle reveals that the extreme value of the energy functional of a system is equivalent to the governing equations and the corresponding boundary conditions. Therefore, the solutions for boundary value problems can be obtained both from partial differential equations in a strict form and the stationary value of the corresponding energy functional in terms of a weak formulation. In this section, as a discretization procedure, the finite element method will be deduced from a generalized variational principle of the elasticity of QCs.

In Ref. [10], Fan has generalized the minimum potential energy principle of classical elasticity to describe the elasticity of QCs. For sufficiently smooth boundaries, if u_i and w_i satisfy Eqs. (1) and (11), then the energy functional of QCs[10] reads

$$\begin{aligned} \Pi &= \int_\Omega F\,{\rm d}\Omega-\int_\Omega (f_iu_i+g_iw_i)\,{\rm d}\Omega \\ &\quad -\int_{\Gamma_{\rm t}}(T_iu_i+h_iw_i)\,{\rm d}\Gamma, \end{aligned} \tag{12}$$

where F is defined as

$$\begin{cases} F=\displaystyle\int_0^{\varepsilon_{ij}}\sigma_{ij}\,{\rm d}\varepsilon_{ij}+\int_0^{w_{ij}}H_{ij}\,{\rm d}w_{ij}=F_{\rm u}+F_{\rm w}+F_{\rm uw}, \\ F_{\rm u}=\dfrac{1}{2}C_{ijkl}\varepsilon_{ij}\varepsilon_{kl}, \\ F_{\rm w}=\dfrac{1}{2}K_{ijkl}w_{ij}w_{kl}, \\ F_{\rm uw}=\dfrac{1}{2}R_{ijkl}\varepsilon_{ij}w_{kl}+\dfrac{1}{2}R'_{ijkl}\varepsilon_{kl}w_{ij}, \end{cases}$$

where R'_{ijkl} is the transpose tensor of R_{ijkl}, and $R'_{ijkl}=R_{klij}$. Equilibrium equation (9) and the stress boundary conditions (10) can be obtained by taking the first variation of Eq. (12). By virtue of the constitutive equation (2), equation (12) can be rewritten as

$$\begin{aligned} \Pi &= \int_\Omega\left(\frac{1}{2}\sigma_{ij}\varepsilon_{ij}+\frac{1}{2}H_{ij}w_{ij}\right){\rm d}\Omega-\int_\Omega(f_iu_i+g_iw_i)\,{\rm d}\Omega \\ &\quad -\int_{\Gamma_{\rm t}}(T_iu_i+h_iw_i)\,{\rm d}\Gamma. \end{aligned} \tag{13}$$

The first variation of the energy functional Π is expressed as

$$\begin{aligned} \delta\Pi &= \int_\Omega(\sigma_{ij}\delta\varepsilon_{ij}+H_{ij}\delta w_{ij})\,{\rm d}\Omega-\int_\Omega(f_i\delta u_i+g_i\delta w_i)\,{\rm d}\Omega \\ &\quad -\int_{\Gamma_{\rm t}}(T_i\delta u_i+h_i\delta w_i)\,{\rm d}\Gamma. \end{aligned} \tag{14}$$

Assuming that the functional Π takes its extreme value, that is, $\delta\Pi=0$, and using Gauss integral theorem, we can rewrite Eq. (14) as

$$\begin{aligned} \delta\Pi &= -\int_\Omega\left[(\partial_j\sigma_{ij}+f_i)\,\delta u_i+(\partial_jH_{ij}+g_i)\,\delta w_i\right]{\rm d}\Omega \\ &\quad +\int_{\Gamma_{\rm t}}\left[(\sigma_{ij}n_j-T_i)\,\delta u_i+(H_{ij}n_j-h_i)\,\delta w_i\right]{\rm d}\Gamma \\ &= 0. \end{aligned}$$

Since δu_i and δw_i are arbitrary and independent variations at region Ω and boundary $\Gamma_{\rm t}$, we have

$$\begin{aligned} &\partial_j\sigma_{ij}+f_i=0,\ \ \partial_jH_{ij}+g_i=0,\ \ (x_1,x_2,x_3)\in\Omega, \\ &\sigma_{ij}n_j-T_i=0,\ \ H_{ij}n_j-h_i=0,\ \ (x_1,x_2,x_3)\in\Gamma_{\rm t}. \end{aligned} \tag{15}$$

Equation (15) equals the equilibrium equation (9) and the stress boundary conditions (10). The second variation of the energy functional Π is

$$\delta^2\Pi = \int_\Omega \left(\frac{1}{2}\frac{\partial^2 F}{\partial \varepsilon_{ij}\partial \varepsilon_{kl}}\delta\varepsilon_{ij}\delta\varepsilon_{kl} + \frac{1}{2}\frac{\partial^2 F}{\partial w_{ij}\partial w_{kl}}\delta w_{ij}\delta w_{kl} + \frac{1}{2}\frac{\partial^2 F}{\partial \varepsilon_{ij}\partial w_{kl}}\delta\varepsilon_{ij}\delta w_{kl} + \frac{1}{2}\frac{\partial^2 F}{\partial w_{ij}\partial \varepsilon_{kl}}\delta w_{ij}\delta\varepsilon_{kl} \right) \mathrm{d}\Omega, \tag{16}$$

where

$$C_{ijkl} = \frac{\partial^2 F}{\partial \varepsilon_{ij}\partial \varepsilon_{kl}}, \quad K_{ijkl} = \frac{\partial^2 F}{\partial w_{ij}\partial w_{kl}},$$
$$R_{ijkl} = \frac{\partial^2 F}{\partial \varepsilon_{ij}\partial w_{kl}}, \quad R_{klij} = R'_{ijkl} = \frac{\partial^2 F}{\partial w_{ij}\partial \varepsilon_{kl}}.$$

According to Eqs. (2), and (5)–(7), equation (16) can be rewritten as

$$\delta^2\Pi = \int_\Omega \frac{1}{2}\delta\left\{\varepsilon_{ij}, w_{ij}\right\}[\boldsymbol{D}]\,\delta\begin{pmatrix}\varepsilon_{ij}\\ w_{ij}\end{pmatrix}\mathrm{d}\Omega. \tag{17}$$

Since $\frac{1}{2}\delta\left\{\varepsilon_{ij}, w_{ij}\right\}[\boldsymbol{D}]\,\delta\begin{pmatrix}\varepsilon_{ij}\\ w_{ij}\end{pmatrix}$ is like the strain energy density of QCs,[29] which is always positive, we can obtain the following relation:

$$\delta^2\Pi > 0,$$

which ensures that $\delta\Pi = 0$ takes not only an extreme value, but also the minimum value of the energy functional.

As a discretization procedure, the finite element method is applied to solve the variational equation and the domain Ω. By dividing the QC body into M sub-domains or elements $\Omega^{(m)}$, we have $\Omega = \sum_{m=1}^{M}\Omega^{(m)}$, where the superscript m is the element number ($m = 1, 2, \ldots, M$). In the arbitrary domain $\Omega^{(m)}$, displacements $u_i^{(m)}$ and $w_i^{(m)}$ can be expressed as

$$\begin{cases} u_i^{(m)} = \sum_{\alpha=1}^{n} I_\alpha u_{i\alpha}^{(m)}, \\ w_i^{(m)} = \sum_{\alpha=1}^{n} I_\alpha w_{i\alpha}^{(m)}, \end{cases} \quad (x_1, x_2, x_3) \in \Omega^{(m)}, \tag{18}$$

where the subscript α is the node number, n is the total number of nodes in the $m-$th element, I_α is the α-th nodal interpolation function, $u_{i\alpha}^{(m)}$ and $w_{i\alpha}^{(m)}$ are, respectively, the phonon and phason displacement fields at the node α in the m-th element. At the inter-element boundaries, the displacements are continuous; that is,

$$\begin{cases} u_i^{(m)} = u_i^{(m')}, \\ w_i^{(m)} = w_i^{(m')}, \end{cases} \quad (x_1, x_2, x_3) \in \Gamma^{(mm')}, \tag{19}$$

where $\Gamma^{(mm')}$ represents the interface between elements m and m'. At the displacement boundary Γ_{u}, the displacements should satisfy the boundary conditions (11).

Under these conditions, the discrete form of the energy functional Π in Eq. (13) can be written as

$$\Pi^* = \sum_{m=1}^{M}\left[\int_{\Omega^{(m)}}\left(\frac{1}{2}\sigma_{ij}^{(m)}\varepsilon_{ij}^{(m)} + \frac{1}{2}H_{ij}^{(m)}w_{ij}^{(m)} - f_i^{(m)}u_i^{(m)} - g_i^{(m)}w_i^{(m)}\right)\mathrm{d}\Omega - \int_{\Gamma_{\mathrm{t}}^{(m)}}\left(T_i^{(m)}u_i^{(m)} + h_i^{(m)}w_i^{(m)}\right)\mathrm{d}\Gamma\right]. \tag{20}$$

By virtue of Eqs. (2), and (5)-(7), equation (20) can be transformed into

$$\Pi^* = \sum_{m=1}^{M}\left\{\int_{\Omega^{(m)}}\left[\frac{1}{2}\left\{\varepsilon_{ij}, w_{ij}\right\}^{(m)}[\boldsymbol{D}]\begin{pmatrix}\varepsilon_{ij}\\ w_{ij}\end{pmatrix}^{(m)} - f_i^{(m)}u_i^{(m)} - g_i^{(m)}w_i^{(m)}\right]\mathrm{d}\Omega - \int_{\Gamma_{\mathrm{t}}^{(m)}}\left(T_i^{(m)}u_i^{(m)} + h_i^{(m)}w_i^{(m)}\right)\mathrm{d}\Gamma\right\}. \tag{21}$$

The displacements in m-th element are consequently written as a column matrix

$$\left\{\bar{u}^{(m)}\right\}^{\mathrm{T}} = \left\{u_1, u_2, u_3, w_1, w_2, w_3\right\}^{(m)}. \tag{22}$$

According to Eq. (1), the strain vector in the m-th element can be written as

$$\begin{pmatrix}\varepsilon_{ij}\\ w_{ij}\end{pmatrix}^{(m)} = [\boldsymbol{L}]\left\{\bar{u}^{(m)}\right\}, \tag{23}$$

where $[\boldsymbol{L}]$ is the element strain differential operator matrix; that is,

$$[\boldsymbol{L}]^{\mathrm{T}} = \begin{bmatrix} \partial_1 & 0 & 0 & 0 & \partial_3 & \partial_2 & 0 & 0 & 0 & 0 & 0 & 0 & 0 & 0 & 0 \\ 0 & \partial_2 & 0 & \partial_3 & 0 & \partial_1 & 0 & 0 & 0 & 0 & 0 & 0 & 0 & 0 & 0 \\ 0 & 0 & \partial_3 & \partial_2 & \partial_1 & 0 & 0 & 0 & 0 & 0 & 0 & 0 & 0 & 0 & 0 \\ 0 & 0 & 0 & 0 & 0 & 0 & \partial_1 & 0 & 0 & 0 & 0 & \partial_2 & 0 & \partial_3 & 0 \\ 0 & 0 & 0 & 0 & 0 & 0 & 0 & \partial_2 & 0 & \partial_3 & 0 & 0 & 0 & 0 & \partial_1 \\ 0 & 0 & 0 & 0 & 0 & 0 & 0 & 0 & \partial_3 & 0 & \partial_1 & 0 & \partial_2 & 0 & 0 \end{bmatrix}. \tag{24}$$

By substituting Eq. (23) into Eq. (21), the resulting equation can be written as

$$\Pi^* = \sum_{m=1}^{M}\left\{\int_{\Omega^{(m)}}\frac{1}{2}\{\bar{u}^{(m)}\}^{\mathrm{T}}[\boldsymbol{L}]^{\mathrm{T}}[\boldsymbol{D}][\boldsymbol{L}]\{\bar{u}^{(m)}\}\mathrm{d}\Omega - \{\bar{u}^{(m)}\}^{\mathrm{T}}\left[\int_{\Omega^{(m)}}\begin{pmatrix}f^{(m)}\\ g^{(m)}\end{pmatrix}\mathrm{d}\Omega + \int_{\Gamma_{\mathrm{t}}^{(m)}}\begin{pmatrix}T^{(m)}\\ h^{(m)}\end{pmatrix}\mathrm{d}\Gamma\right]\right\}. \tag{25}$$

In the m-th element, the element displacement vector $\{\bar{u}^{(m)}\}$ can be determined by the nodal displacements as

$$\left\{\bar{u}^{(m)}\right\} = [I]\left\{\tilde{u}^{(m)}\right\}, \tag{26}$$

where $[\boldsymbol{I}] = \{[\boldsymbol{I}_1], [\boldsymbol{I}_2], \ldots, [\boldsymbol{I}_\alpha], \ldots, [\boldsymbol{I}_n]\}$ is the element inter-

polation matrix with

$$[\boldsymbol{I}_\alpha] = \begin{bmatrix} I_\alpha & 0 & 0 & 0 & 0 & 0 \\ 0 & I_\alpha & 0 & 0 & 0 & 0 \\ 0 & 0 & I_\alpha & 0 & 0 & 0 \\ 0 & 0 & 0 & I_\alpha & 0 & 0 \\ 0 & 0 & 0 & 0 & I_\alpha & 0 \\ 0 & 0 & 0 & 0 & 0 & I_\alpha \end{bmatrix}. \tag{27}$$

$\{\tilde{u}^{(m)}\} = \{\{\tilde{u}_1^{(m)}\}, \{\tilde{u}_2^{(m)}\}, \ldots, \{\tilde{u}_\alpha^{(m)}\}, \ldots, \{\tilde{u}_n^{(m)}\}\}^{\mathrm{T}}$ represents all nodal displacements in the m-th element and $\{\tilde{u}_\alpha^{(m)}\}$ is a six-dimensional displacement vector denoting the displacement components of the node α; that is,

$$\left\{\tilde{u}_\alpha^{(m)}\right\}^{\mathrm{T}} = \{u_{1\alpha}, u_{2\alpha}, u_{3\alpha}, w_{1\alpha}, w_{2\alpha}, w_{3\alpha}\}^{(m)}.$$

The body force in the m-th element can be denoted as

$$\begin{pmatrix} f^{(m)} \\ g^{(m)} \end{pmatrix} = \left\{\left\{\tilde{f}_1^{(m)}\right\}, \left\{\tilde{f}_2^{(m)}\right\}, \ldots, \left\{\tilde{f}_\alpha^{(m)}\right\}, \ldots \left\{\tilde{f}_n^{(m)}\right\}\right\}^{\mathrm{T}},$$

and

$$\left\{\tilde{f}_\alpha^{(m)}\right\}^{\mathrm{T}} = \{f_{1\alpha}, f_{2\alpha}, f_{3\alpha}, g_{1\alpha}, g_{2\alpha}, g_{3\alpha}\}^{(m)}.$$

The traction is

$$\begin{pmatrix} T^{(m)} \\ h^{(m)} \end{pmatrix} = \left\{\left\{\tilde{T}_1^{(m)}\right\}, \left\{\tilde{T}_2^{(m)}\right\}, \cdots, \left\{\tilde{T}_\alpha^{(m)}\right\}, \cdots \left\{\tilde{T}_n^{(m)}\right\}\right\}^{\mathrm{T}},$$

and

$$\left\{\tilde{T}_\alpha^{(m)}\right\}^{\mathrm{T}} = \{T_{1\alpha}, T_{2\alpha}, T_{3\alpha}, h_{1\alpha}, h_{2\alpha}, h_{3\alpha}\}^{(m)}.$$

By applying $\delta\Pi^* = 0$ to Eq. (25), we obtain the following algebraic system of equations:

$$[\boldsymbol{A}]\{\tilde{u}\} = [\boldsymbol{F}], \tag{28}$$

where

$$[\boldsymbol{A}] = \sum_{m=1}^{M} \int_{\Omega^{(m)}} [\boldsymbol{B}]^{\mathrm{T}} [\boldsymbol{D}][\boldsymbol{B}] \mathrm{d}\Omega, \quad [\boldsymbol{B}_\alpha] = [\boldsymbol{L}][\boldsymbol{I}_\alpha],$$

$$[\boldsymbol{F}] = \sum_{m=1}^{M} \left\{ \int_{\Omega^{(m)}} [\boldsymbol{I}]^{\mathrm{T}} \begin{pmatrix} f^{(m)} \\ g^{(m)} \end{pmatrix} \mathrm{d}\Omega + \int_{\Gamma_{\mathrm{t}}^{(m)}} [\boldsymbol{I}]^{\mathrm{T}} \begin{pmatrix} T^{(m)} \\ h^{(m)} \end{pmatrix} \mathrm{d}\Gamma \right\}, \tag{29}$$

and $\{\tilde{u}\} = \{\{\tilde{u}^{(1)}\}, \{\tilde{u}^{(2)}\}, \ldots, \{\tilde{u}^{(N)}\}\}^{\mathrm{T}}$ is the displacement vector of all nodes in the domain Ω, where N is the total number of nodes. The strain fields will be obtained by applying Eq. (23) to the displacements $\{\tilde{u}\}$, which are derived by solving Eq. (28). The stress fields of icosahedral QC in the m-th element can be evaluated at the Gauss integral points through the element node displacement components, as follows:

$$\begin{pmatrix} \sigma_{ij} \\ H_{ij} \end{pmatrix}^{(m)} = [\boldsymbol{D}][\boldsymbol{B}] \left\{\tilde{u}^{(m)}\right\}. \tag{30}$$

In our computation, we use 8-node or 20-node brick elements exhibiting linear or quadratic shape functions and 27 Gaussian points to perform the integration in Eq. (29). In the following, we first give analytical and numerical solutions for an icosahedral Al–Pd–Mn QC cuboid subjected to a uniaxial tension to verify the accuracy of our procedure. Then, a cracked icosahedral Al–Pd–Mn QC plate with a finite size under the Mode-I loading is numerically analyzed to reveal the fracture behavior of the matter. It should be noted that in the studies of the two specimens, the body forces in Eq. (29) are ignored.

4. An icosahedral Al–Pd–Mn QC cuboid subjected to a uniaxial tension

We consider a 3D icosahedral Al–Pd–Mn QC cuboid with a height of H subjected to a uniaxial tensile force F (see Fig. 1). The Cartesian coordinate system (x_1, x_2, x_3) is introduced with the bottom and top surfaces lying in the planes $x_3 = 0$ and $x_3 = H$, respectively. The coordinate origin is located at the center of the bottom of the cuboid. The area of the cross section of the cuboid is L^2.

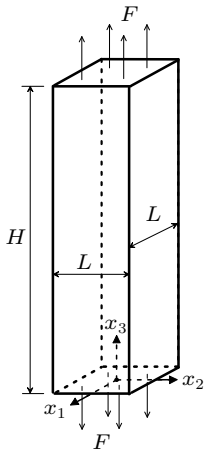


Fig. 1. An icosahedral QC cuboid subjected to a uniaxial tension.

According to the loading of the cuboid, the stress components are

$$\sigma_{33} = \frac{F}{L^2}, \ \sigma_{11} = \sigma_{22} = \sigma_{23} = \sigma_{31} = \sigma_{12} = 0, \ H_{ij} = 0. \tag{31}$$

Inserting Eq. (31) into Eq. (7) leads to the following strain components in the x_3 direction:

$$\varepsilon_{11} = \varepsilon_{22} = \frac{-F\left(\lambda + \dfrac{2R^2}{K_1+K_2}\right)}{2L^2\left[2\mu^2 + 3\lambda\mu - \dfrac{R^2(9\lambda+6\mu)}{K_1+K_2}\right]},$$

$$\varepsilon_{33} = \frac{F\left(\lambda + \mu - \dfrac{R^2}{K_1+K_2}\right)}{L^2\left[2\mu^2 + 3\lambda\mu - \dfrac{R^2(9\lambda+6\mu)}{K_1+K_2}\right]},$$

$$w_{33} = \frac{FR}{L^2\left[\mu(K_1+K_2) - 3R^2\right]}, \quad \varepsilon_{ij} = w_{ij} = 0 \ (i \neq j). \tag{32}$$

The displacement boundary conditions for this problem can be written as

$$u_3 = w_3 = 0, \quad \text{for} \quad x_3 = 0;$$
$$u_1 = u_2 = w_1 = w_2 = 0, \quad \text{for} \quad x_1 = x_2 = x_3 = 0. \quad (33)$$

According to Eqs. (32) and (33), the corresponding displacements of the cuboid are

$$u_1 = \frac{-F\left(\lambda + \dfrac{2R^2}{K_1+K_2}\right)x_1}{2L^2\left[2\mu^2 + 3\lambda\mu - \dfrac{R^2(9\lambda+6\mu)}{K_1+K_2}\right]},$$
$$u_2 = \frac{-F\left(\lambda + \dfrac{2R^2}{K_1+K_2}\right)x_2}{2L^2\left[2\mu^2 + 3\lambda\mu - \dfrac{R^2(9\lambda+6\mu)}{K_1+K_2}\right]},$$
$$u_3 = \frac{F\left(\lambda + \mu - \dfrac{R^2}{K_1+K_2}\right)x_3}{L^2\left[2\mu^2 + 3\lambda\mu - \dfrac{R^2(9\lambda+6\mu)}{K_1+K_2}\right]},$$
$$w_3 = \frac{FRx_3}{L^2(\mu K_1 + \mu K_2 - 3R^2)}. \quad (34)$$

If there is no phonon–phason coupling effect, that is, $R = 0$, then Eq. (34) can be reduced to

$$u_1 = \frac{-F\lambda x_1}{2L^2(2\mu^2 + 3\lambda\mu)}, \quad u_2 = \frac{-F\lambda x_2}{2L^2(2\mu^2 + 3\lambda\mu)},$$
$$u_3 = \frac{F(\lambda+\mu)x_3}{L^2(2\mu^2 + 3\lambda\mu)}, \quad w_3 = 0, \quad (35)$$

which coincides with the displacements from the classical elasticity of crystal.

Next, the displacements calculated numerically are compared with the analytical results. The material parameters of a 3D icosahedral Al–Pd–Mn QC are given by[12–15]

$$\lambda = 74.9\ \text{GPa}, \quad \mu = 72.4\ \text{GPa}, \quad K_1 = 72\ \text{MPa}, \quad K_2 = -37\ \text{MPa}.$$

The coupling constant R of the Al–Pd–Mn QC has not yet been measured. In the computations, we assume that $R/\mu = 0$, 0.001, 0.002, 0.004, 0.006, 0.008, and 0.01. The height H of the cuboid is 4 cm, and the area of the cross section is $L^2 = 1\ \text{cm}^2$. The tensile force F is 1 kN. The calculated domain is meshed by 32 $0.5 \times 0.5 \times 0.5\ \text{cm}^3$ 8-node hexahedron elements.

The displacements of the point (0.5, 0.5, 4) at the top surface of the cuboid are shown in Table 1. The results show that the numerical solutions are the same as the analytical ones. As R/μ increases, the absolute values of displacements u_1, u_3 and w_3 increase. For $R/\mu = 0.01$, the displacement w_3 is about six times greater than u_3, demonstrating the coupling effect of this QC. Certainly, the influence of R/μ on the displacements in the phonon field depends on K_1 and K_2.

Table 1. Comparison between the displacements (10^{-2} cm) of the point (0.5, 0.5, 4).

R/μ	u_1		u_2		w_3	
	analytical	numerical	analytical	numerical	analytical	numerical
0	−0.00070	−0.00070	0.02202	0.02202	0	0.00000
0.001	−0.00071	−0.00071	0.02214	0.02214	0.11500	0.11500
0.002	−0.00073	−0.00073	0.02249	0.02249	0.23439	0.23439
0.004	−0.00083	−0.00083	0.02405	0.02405	0.50754	0.50754
0.006	−0.00103	−0.00103	0.02732	0.02732	0.88298	0.88298
0.008	−0.00146	−0.00146	0.03416	0.03416	1.51665	1.51665
0.01	−0.00258	−0.00258	0.05215	0.05215	3.01205	3.01205

The displacements along the loading axis, with x_1 or x_2 serving as the tensile axis (see Fig. 2), are briefly given below.

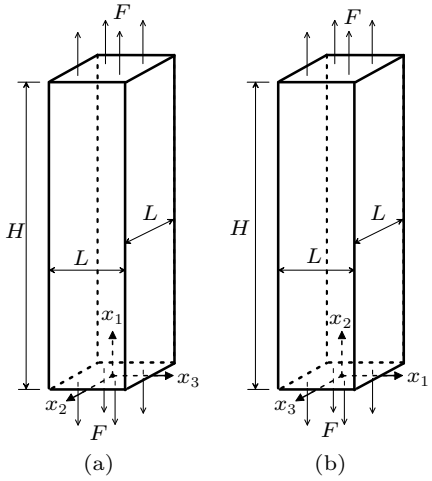


Fig. 2. An icosahedral QC cuboid with x_1 or x_2 as the tensile axis.

(a) When x_1 is the tensile axis, there are

$$u_1 = \frac{F\left(\lambda + \mu - \dfrac{R^2}{K_1+K_2}\right)x_1}{L^2\left[2\mu^2 + 3\lambda\mu - \dfrac{R^2(9\lambda+6\mu)}{K_1+K_2}\right]},$$
$$w_1 = -\frac{FRx_1}{2L^2(\mu K_1 + \mu K_2 - 3R^2)}. \quad (36)$$

(b) When x_2 is the tensile axis, there are

$$u_2 = \frac{F\left(\lambda + \mu - \dfrac{R^2}{K_1+K_2}\right)x_2}{L^2\left[2\mu^2 + 3\lambda\mu - \dfrac{R^2(9\lambda+6\mu)}{K_1+K_2}\right]},$$
$$w_2 = \frac{FRx_2}{2L^2(\mu K_1 + \mu K_2 - 3R^2)}. \quad (37)$$

It can be seen that the phonon displacements are the same for all three kinds of tensile axes, whereas the phason displacements are different from each other. This reveals the 3D anisotropic characteristics of the icosahedral QC. For simplicity, the numerical verifications of Eqs. (36) and (37) are not presented in this paper.

To study the mechanical behavior of the icosahedral Al–Pd–Mn QC, a cracked thin plate with a finite size under Mode–I loading are investigated with our numerical method.

5. Fracture behavior study of a cracked icosahedral Al–Pd–Mn QC plate with a finite size under Mode–I loading

An icosahedral Al–Pd–Mn QC plate containing a penetrating crack subjected to a uniform tensing load P is shown in Fig. 3, where $a = 5$ mm, $H = 50$ mm, $L = 60$ mm, and $P/\mu = 0.001$. The thickness of the plate is 1 mm, which is 10% of the crack length $2a$ and 1% of the plate height $2H$. The point O is the coordinate origin, and the front and back faces of the plate are within the planes $x_3 = 0$ and $x_3 = -1$ mm. The elastic constants of the QC are the same as those in Section 4. We assume $R/\mu = 0.005$ for the coupling case, and $R/\mu = 0$ for the decoupling case.

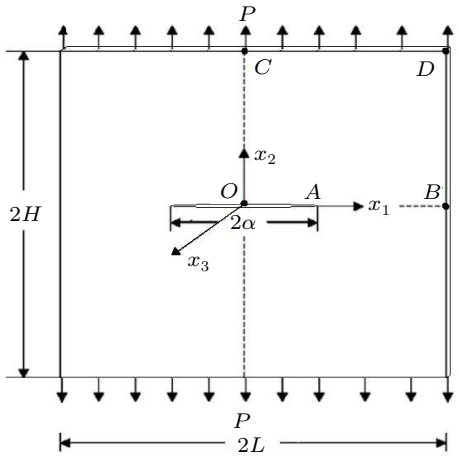


Fig. 3. Icosahedral QC plate with a crack under Mode-I loading.

Due to the symmetry of the specimen, only the top-right 1/4 part ($0 \le x_1 \le L, 0 \le x_2 \le H, -1$ mm $\le x_3 \le 0$) needs to be modeled. The following boundary conditions must be satisfied:

$$
\begin{aligned}
&a \le x_1 \le L, x_2 = 0\text{: } u_2 = 0, w_2 = 0;\\
&x_1 = 0, 0 \le x_2 \le H\text{: } u_1 = 0, w_1 = 0;\\
&x_3 = -0.5\text{ mm}\text{: } u_3 = 0, w_3 = 0;\\
&0 \le x_1 \le L, x_2 = H\text{: } \sigma_{22} = P,\\
&\qquad\qquad \text{other } \sigma_{ij}n_j = 0 \text{ and } H_{ij}n_j = 0;\\
&0 \le x_1 \le a, x_2 = 0\text{: } \sigma_{ij}n_j = 0 \text{ and } H_{ij}n_j = 0;\\
&x_1 = L, 0 \le x_2 \le H\text{: } \sigma_{ij}n_j = 0 \text{ and } H_{ij}n_j = 0;\\
&x_3 = 0 \text{ and } -1\text{ mm}\text{: } \sigma_{ij}n_j = 0 \text{ and } H_{ij}n_j = 0,
\end{aligned}
\tag{38}
$$

with the unit normal vector n_j being at the boundaries. The domain $0 \le x_1 \le L, 0 \le x_2 \le H, -1$ mm $\le x_3 \le 0$ is meshed by 3D 20-node hexahedron elements with a thickness of 1 mm along the x_3 axis. The finite element model is shown in Fig. 4. There are 766 elements and 5775 nodes. A layer of elements, 0.1 mm in height, is placed at the bottom of the model in order to conveniently analyze the stress intensity factor of the crack. The zone around the crack is meshed by elements, with 0.1 mm in height and 0.1 mm in width, and the width is 2% of the crack length a. To model the displacements and stresses near the crack tip accurately, the elements related to the crack tip are degenerated in terms of singular quarter–point brick elements.[30,31]

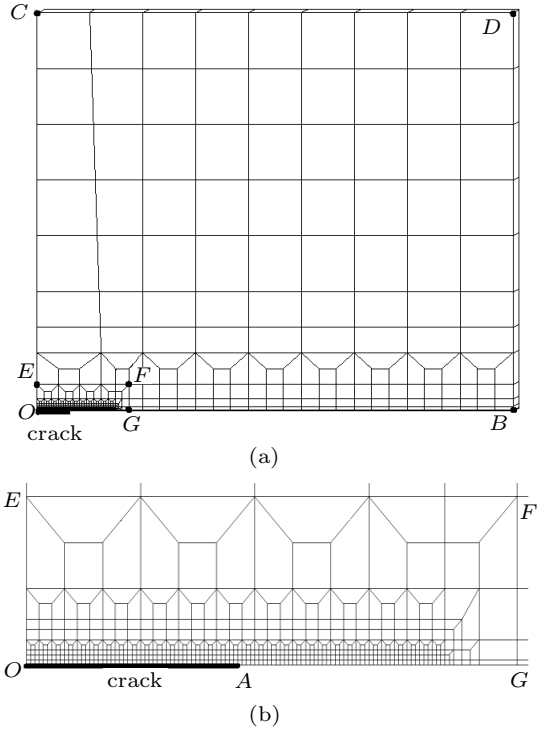


Fig. 4. Finite element model of the specimen.

Because the plate thickness is very small compared with the height and width of the plate, and the load P is parallel to the x_1–x_2 plane, the differences between the stresses in the Gauss integral points of the finite element model along the x_3 direction are very small. Therefore, the stresses will be averaged along the x_3 axis.

The values of the normal phonon stress ratio σ_{22}/P at the integration points of the element layer in the crack plane are given in Fig. 5, with $r = \sqrt{(x_1 - a)^2 + x_2^2}$. The normal stress ratio at the crack tip is 35.667 for $R/\mu = 0.005$, while it is 34.187 for $R/\mu = 0$. With the increase in the ratio r/a, the stress ratios for the two cases rapidly come close to each other, finally approaching 1.0; thereby, satisfying the stress boundary conditions (38).

The decoupling of stress fields on the ligament ($x_2 = 0, a < |x_1| < L$) is well known in linear elastic and piezoelectric fracture mechanics.[32] The contours of the normal stress ratio σ_{22}/P for $R/\mu = 0.005$ are shown in Fig. 6. It can be

seen that there is a stress concentration at the crack tip line. At a distant position from the crack, the stress ratio approaches 1.0, once again demonstrating the consistency with the stress boundary conditions (38).

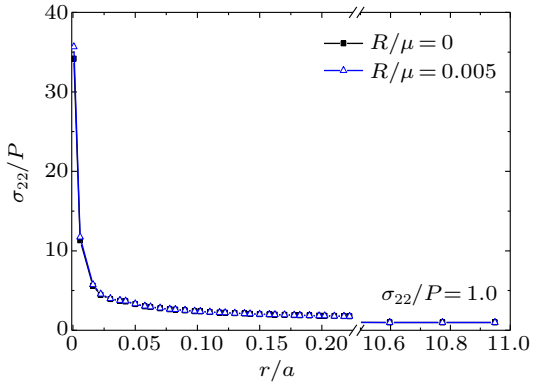


Fig. 5. (color online) Normal phonon stress ratio σ_{22}/P versus r/a.

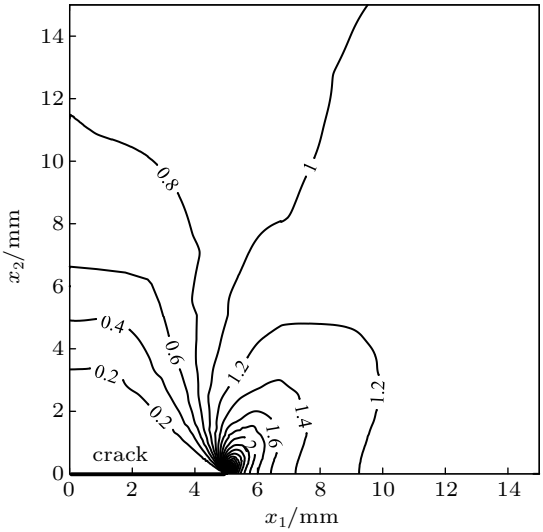


Fig. 6. Contours of normalized phonon stress σ_{22}/P near the crack tip for $R/\mu = 0.005$.

To characterize the crack-tip loading, the stress intensity factors are well established for the linear fracture problems. Following Refs. [10] and [33], the phonon stress intensity factor for a Mode-I crack yields

$$K^{\mathrm{II}} = \lim_{x_1 \to a^+} \left[\sqrt{2\pi (x_1 - a)} \sigma_{22}(x_1, 0) \right] = f(a/L) \sqrt{\pi a} P, \quad (39)$$

on the assumption that $R^2/(\mu K_1) \leq 1$, where $f(a/L)$ characterizes the geometry factor of a specimen with a finite size. In other words, for different specimen geometries, there will be different values of f. Up to now, the expression of f for the crack problem of the icosaheral QC has not been given in literatures. Therefore, it is necessary to use a numerical method to calculate the stress intensity factors of various specimens. The first term on the right-hand side of Eq. (39) is always used to determine the stress intensity factor numerically for the crack problems of specimens with a finite size. We will use the term of Eq. (39) to determine the stress intensity factor of this specimen.

An extrapolation method based on the stress σ_{22} at the element Gauss integration points is applied to calculate the stress intensity factors from numerical solutions. The stresses at the Gauss points of elements in the front of the crack tip and adjacent to the crack plane are almost identical to the stresses at $x_2 = 0$. With the position x_{1s} of the corresponding normal stress $(\sigma_{22})_s$ and $r_s = x_{1s} - a$, K_s^{II} reads

$$K_s^{\mathrm{II}} = \sqrt{2\pi r_s} (\sigma_{22})_s, \quad (40)$$

where the subscript s denotes the number of the Gauss points. If we choose Q Gauss points, then $s = 1, 2, \ldots Q$. Figure 7 shows the relationships between K_s^{II} and r_s for $R/\mu = 0$ and $R/\mu = 0.005$. It is shown that the stress intensity factors K_s^{II} for $R/\mu = 0.005$ are almost identical to those for $R/\mu = 0$. Near the crack tip, the results are inaccurate due to the singularity while approaching a straight line as r_s increases. Therefore, we can apply the least-squares method to solve the values of the straight lines. Finally, the stress intensity factor K^{II} is obtained as the intersection of the straight line with the ordinate axis, which can be calculated as follows:

$$K^{\mathrm{II}} \approx \frac{\sum r_s \sum r_s K_s^{\mathrm{II}} - \sum r_s^2 \sum K_s^{\mathrm{II}}}{(\sum r_s)^2 - Q \sum r_s^2}. \quad (41)$$

The Gauss points in the domain $0.5 < r_s < 3$ are chosen to determine the stress intensity factor K^{II} and further $Q = 76$. The intensity factors for the two cases are obtained to be 290.61 and 290.21 MPa·mm$^{1/2}$ for $R/\mu = 0$ and $R/\mu = 0.005$, respectively. By substituting $a = 5$ mm and $P/\mu = 0.001$ into Eq. (39), the stress intensity factor is obtained to be $286.95f$ MPa·mm$^{1/2}$. The numerical solutions of the geometry factor f for $R/\mu = 0$ and $R/\mu = 0.005$ are 1.013 and 1.011, respectively.

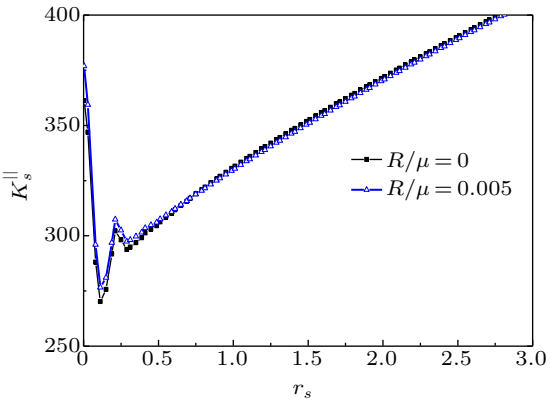


Fig. 7. (color online) Stress intensity factor K_s^{II} from different Gauss points versus $r_s = x_{1s} - a$.

Figure 8 depicts the opening displacement u_2 of the crack at OA in the plane $x_3 = 0$. This shows that the crack opening

displacement for $R/\mu = 0.005$ is larger than that for $R/\mu = 0$. At $x_1 = 0$, the opening displacement for $R/\mu = 0.005$ is 0.00441 mm, and $u_2 = 0.00402$ mm for $R/\mu = 0$. It can be seen that the crack opening is obviously influenced by the coupling between the phonon and phason fields.

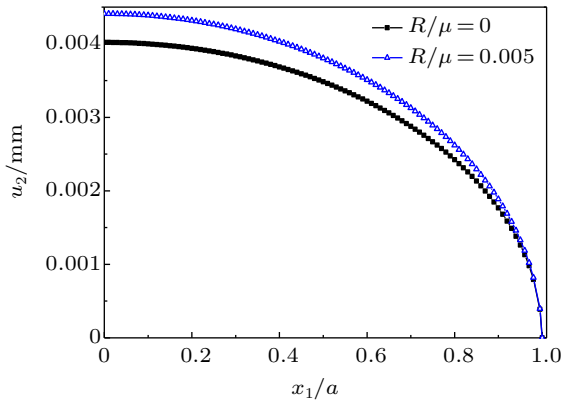


Fig. 8. (color online) Opening displacement u_2 of the crack at OA in the plane $x_3 = 0$.

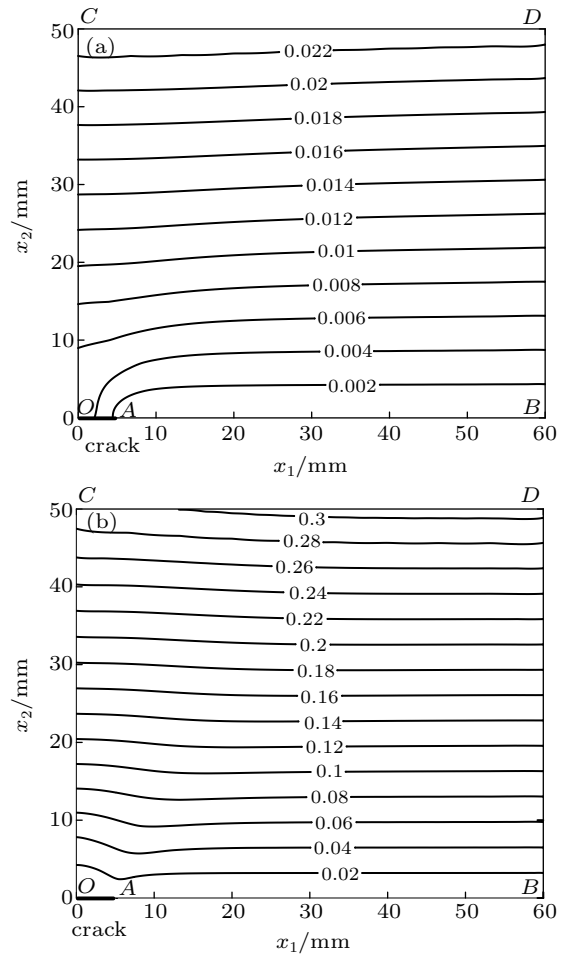


Fig. 9. Contours of normal (a) phonon and (b) phason displacements u_2 and w_2 for $R/\mu = 0.005$ in the plane $x_3 = 0$.

The contours of the normal displacements u_2 and w_2 in the plane $x_3 = 0$ are shown for $R/\mu = 0.005$ in Fig. 9. The existence of the crack increases the phonon displacement and reduces the phason displacement, unlike the case where the plate has no such crack. Furthermore, in the horizontal direction, the displacement changes are small at distant positions from the crack. The displacement w_2 is more than ten times greater than u_2. At the point D, the displacements u_2 and w_2 are 0.02288 and 0.30636 mm, respectively. The displacements at BD (at $x_1 = 60$ mm) should be almost consistent with analytical displacements for the plate with no such crack, which can be obtained from Eq. (37). According to Eq. (37), the corresponding analytical displacements are 0.02299 and 0.30653 mm. Compared with the analytical results, the errors of our calculated displacements u_2 and w_2 at the point D are -0.5% and 0.1%. This further corroborates the correctness of our calculated displacement fields. Figure 9 also shows the coupling influence between the phonon and phason field, bearing in mind that there is no load exerted on the phason field.

Figures 5–9 show that the coupling effect between the phonon and phason fields has a strong influence on the displacement field, but a very weak influence on the stress field. This phenomenon is due to the method of loading in our study.

6. Conclusions

Based on the variation of the energy functional of the elasticity of QCs and discretization, a 3D finite element formulation for the icosahedral QCs is developed. The reliability of this procedure is verified by an Al–Pd–Mn cuboid subjected to a uniaxial tension. In the investigation of this specimen, the analytical solutions are given. From the comparisons of the analytical and numerical results between different phonon–phason coupling parameters, it can be seen that the numerical solutions are consistent with the analytical results. Then, a thin plate of an icosahedral Al–Pd–Mn QC containing a crack subjected to Mode–I loading is investigated. Different cases (both with and without phonon–phason coupling) are considered. In addition, the geometry factors are calculated, including the stress intensity factor and the crack opening displacement. The results regarding the two specimens show an evident coupling effect of the icosahedral Al–Pd–Mn QC.

The accuracy and efficiency of our numerical method have been proved. Therefore, the procedure can be used to solve more complicated boundary value problems and can be extended to more sophisticated methods for crack-tip loading analysis.

References

[1] Shechtman D, Blech I, Gratias D and Cahn J W 1984 *Phys. Rev. Lett.* **53** 1951
[2] Levine D and Stcinhardt P J 1984 *Phys. Rev. Lett.* **53** 2477
[3] Ronchetti A M and Tasker P W 1987 *Phil. Mag.* **56** 237
[4] Ovid'ko I A 1992 *Mat. Sci. Eng.: A* **154** 29
[5] Wollgarten M, Beyss M, Urban K, Liebertz H and Köster U 1993 *Phys. Rev. Lett.* **71** 549

[6] Ma J Y, Wang J B and Wang R H 2008 *J. Phys. D: Appl. Phys.* **41** 085413
[7] Bak P 1985 *Phys. Rev. Lett.* **54** 1517
[8] Bak P 1985 *Phys. Rev. B* **32** 5764
[9] Levine D, Lubensky T C, Qstlund S, Ramaswamy S and Steinhardt P J 1985 *Phys. Rev. Lett.* **54** 1520
[10] Fan T Y 2011 *Mathematical Theory of Elasticity of Quasicrystals and Its Applications* (Heidelberg: Springer)
[11] Ding D H, Yang W G, Hu C Z and Wang R H 1993 *Phys. Rev. B* **48** 7003
[12] Letoublon A, de Boissien M, Boudard M, Mancini L, Gastaldi J, Hennion B, Caudron R and Bellissent R 2001 *Phil. Mag. Lett.* **81** 273
[13] Capitan M J, Calvayrac Y, Quivy A, Joulaud J L, LeFebvre S and Gratias D 1999 *Phys. Rev. B* **60** 6398
[14] Tanaka K, Mitarai Y and Koiwa M 1996 *Phil. Mag. A* **76** 1715
[15] Edagawa K and So GY 2007 *Phil. Mag.* **87** 77
[16] Bachteler J and Trebin H R 1998 *Eur. Phys. J. B* **4** 299
[17] Gao Y and Ricoeur A 2010 *Phys. Lett. A* **374** 4354
[18] Zhu A Y and Fan T Y 2007 *Chin. Phys.* **16** 1111
[19] Gao Y, Ricoeur A and Zhang L L 2011 *Phys. Lett. A* **375** 2775
[20] Chen W Q, Ma L and Ding H J 2004 *Mech. Res. Commun.* **31** 633
[21] Fan T Y and Peng Y Z 2000 *Chin. Phys. B* **9** 764
[22] Li L H and Fan T Y 2008 *Sci. China Ser. G* **51** 773
[23] Li L H and Fan T Y 2007 *Phys. Lett. A* **372** 510
[24] Schaaf G D, Roth J, Trebin H R and Mikulla R 2000 *Phil. Mag. A* **80** 1657
[25] Wang X F, Fan T Y and Zhu A Y 2009 *Chin. Phys. B* **18** 709
[26] Sladek J, Sladek V and Pan E 2013 *Int. J. Solids Struct.* **50** 3975
[27] Sladek J, Sladek V, Krahulec S, Zhang Ch and Wünsche M 2013 *Int. J. Fract.* **181** 115
[28] Radi E and Mariano P M 2011 *Math. Meth. Appl. Sci.* **34** 1
[29] Hu C Z, Wang R H and Ding D H 2000 *Rep. Prog. Phys.* **63** 1
[30] Henshell R D and Shaw K G 1975 *Int. J. Num. Meth. Eng.* **9** 495
[31] Barsoum R S 1975 *Int. J. Num. Meth. Eng.* **10** 25
[32] Ricoeur A and Kuna M 2003 *J. Eur. Ceram. Soc.* **23** 1313
[33] Tada H, Paris P C and Irwin G R 1985 *The Stress Analysis of Cracks* (Del Research Corporation)